Multifluid model of a one-dimensional steady state magnetotail current sheet

L. C. Steinhauer,[1] M. P. McCarthy,[2] and E. C. Whipple[2]

Received 31 May 2007; revised 29 November 2007; accepted 19 December 2007; published 10 April 2008.

[1] The central current sheet of the magnetotail has been modeled frequently as a nearly one-dimensional configuration that might have a significant role in magnetospheric physics as a site of particle acceleration. Yet comparisons of data with tail models have mainly used the Harris solution in spite of its deficiencies: No normal magnetic field, uniform cross-tail drift, and vanishing asymptotic plasma density. We present a time-independent one-dimensional multifluid model that separates ions into groups coming from sources above and below the current sheet. Electrons are a separate group. A disadvantage is that equations of state are required for closure. The isotropic pressure equation of state is supported by observation and gives reasonable results. This model is more realistic; it encodes more information than a single fluid or an ion and electron fluid model. This fluid model can be easily used to compare with magnetotail data. Field and plasma moment data provide boundary conditions for a model calculation. We examine symmetric models that predict specific relations between various quantities, such as magnetic field or density. Solutions are obtained similar to Harris' model, but with non-uniform out-of-plane ion flow and non-vanishing asymptotic density. Sheet thickness has weak dependence on the normal magnetic field and modest dependence on electron-to-ion pressure ratio. The ratio of sheet center to asymptotic density decreases with asymptotic ion pressure. This one-dimensional configuration of the current sheet, in Earth's reference frame, provides an example of conversion of electromagnetic energy into fluid energy.

Citation: Steinhauer, L. C., M. P. McCarthy, and E. C. Whipple (2008), Multifluid model of a one-dimensional steady state magnetotail current sheet, *J. Geophys. Res.*, *113*, A04207, doi:10.1029/2007JA012578.

1. Introduction

[2] It has been known for some time that the central current sheet in the magnetotail is a site for particle energization. The sharp change in the tangential component of the magnetic field (B_x) directs particles along the cross-tail electric field (E_y) producing acceleration of both ions and electrons. Early work by *Speiser* [1965a, 1965b, 1967, 1970] used particle trajectories in models of the current sheet with a small E_y and showed acceleration of particles in the non-adiabatic central region where the magnetic moment changes. Ions execute a half-gyration about B_z in the xy-plane as they reverse their motion in the x-direction while they simultaneously oscillate in the z-direction about the midplane. The half-gyration gives the ion an incremental step in the y-direction, and therefore a gain in velocity from E_y. This gain in velocity is directed toward the Earth after ejection from the central sheet. (See Figure 1 by *Lyons* [1984] for a sketch of electron motion (with $E_y = 0$), which resembles the ion motion except it is reversed and has a smaller scale for the gyromotion.) *Lyons and Speiser* [1982] and *Lyons* [1984] found the effects of this acceleration on both ion and electron distribution functions. They suggested that accelerated ions ejected from the current sheet are an important source of auroral ion precipitation.

[3] Work on self-consistent kinetic models of the current sheet was pioneered by *Sestero* [1966] and by *Schindler* [1972, 1975, 1979] who presumed a much larger scale in the plane of the current sheet than in the normal (z) direction. *Kan* [1973] obtained exact solutions for the two dimensional (2-D) tail using a single Maxwellian distribution having uniform drift velocity and also a two component Maxwellian distribution having a sheared drift. His technique has been used by others to obtain 2-D solutions with an X-point (reviewed by *Yoon and Lui* [2005]). *Eastwood* [1972], *Hill* [1975], *Cowley* [1978a, 1978b], *Cowley and Pellat* [1979], *Francfort and Pellat* [1976], and others have discussed both the fluid and kinetic aspects of the current sheet, showing the importance of the balance between magnetic field pressure and the particle pressure component along the magnetic field, $p_{\|}$. A significant aspect of particle energization is that the first adiabatic invariant is conserved through the sheet despite failure of magnetic moment conservation [*Schindler*, 1965; *Sonnerup*, 1969, 1971]. In regions of large gradients, the form of the first adiabatic

[1] Redmond Plasma Physics Laboratory, University of Washington, Redmond, Washington, USA.
[2] Earth and Space Sciences, University of Washington, Seattle, Washington, USA.

0148-0227/08/2007JA012578

invariant differs significantly from the magnetic moment. If an electric field is present, especially a component in the GSM y-direction, particles will gain energy while traversing the sheet center (see section 4). After ejection from the current sheet, the first adiabatic invariant reverts to the magnetic moment, and, if the magnetic field is symmetric about the center, a particle's perpendicular kinetic energy reverts to its incoming value. Thus the added energy appears in the motion component along the magnetic field. More recent work (Birn, Hesse, Sitnov, Zelenyi, and others; reviewed by *Lui* [2004]) has also investigated 1-D models.

[4] *Tsyganenko* [1995, 1998], *Tsyganenko et al.* [1998], *Tsyganenko and Mukai* [2003], and *Tsyganenko and Fairfield* [2004] have constructed models of the tail magnetic field from many spacecraft measurements. While the large central gradient in magnetic field is generated by the local current, the asymptotic behavior is determined by Earth's dipole plus other remote current systems. *Baumjohann et al.* [1988, 1989] used data from AMPTE/IRM to obtain ion moments adjacent to and in the central plasma sheet, and *Baumjohann* [1998] found that density and pressure were often well-correlated, especially during single traversals of the central sheet, supporting an isotropic pressure equation of state with a polytropic index close to 5/3 and an ion to electron temperature ratio near 7.

[5] While a number of studies have attempted to compare spacecraft data obtained in the magnetotail current sheet with models of the sheet, these have mainly used the Harris model [*Harris*, 1962], which we argue is an inappropriate model for comparison [*Thompson et al.*, 2006; *Tsyganenko et al.*, 1998; *Sitnov*, 2006]. Consider several deficiencies of the Harris model: (1) there is no normal field, $B_z = 0$, so that no particles cross the sheet from asymptotic sources; (2) the unrealistic assumption of uniform cross-tail drift velocity, u_y; (3) vanishing particle density far from the sheet; (4) assumption of a simple Maxwellian velocity distribution; (5) further, one study showed that atypical current sheet structures with bifurcated current density occur 17% of the time, and even for typical center-peaked sheets, strongly peaked structures frequently appear in the center, which also differs from the Harris profile [*Asano et al.*, 2005]. We believe that comparisons between measured and model structures across the magnetotail current sheet should be made with a more realistic model.

2. Properties and Advantages of a Multifluid Model

[6] In this paper we propose a steady (time-independent) multifluid model for comparison with measured structures in assumed 1-D magnetotail current sheets. We adopt a multifluid model, despite an increased emphasis on obviously kinetic behaviors evident in recent detailed measurements of plasma distribution functions together with the observations of complicated dynamic behavior of the magnetospheric plasma. An example is the simultaneous appearance of separate beams of ions in different directions with different fluxes. *Parks et al.* [2001] and *Parks* [2004] have pointed out that microphysical processes are key to understanding these new observations that, evidently, are unexplainable by conventional magnetohydrodynamic models. A kinetic approach is, in principle, the most accurate model, but it proves very difficult in practice. In using the kinetic approach, one searches for constants of motion. However, a typical measured distribution function rarely appears as a simple function of velocity. Further, aside from the total energy, constants of motion can be difficult to relate to measured quantities.

[7] The fluid approach has an advantage over a kinetic approach. It is simpler to work with the variables of fluid theory (density, flow velocity, pressure) than with distribution functions. This approach is sound because the fluid variables are available experimentally through their identification with combinations of the moments of measured distribution functions, and because the fluid equations express conservation laws. Two disadvantages of the fluid approach are the loss of information incurred in exchanging distribution functions for a few of their moments, and there are more unknown variables than there are equations. Hence one must achieve closure by choosing equations of state.

[8] Recent papers by *Ueno et al.* [2001] and *Lui et al.* [2005] developed a multicomponent approach in order to provide better insight into the behavior of the different plasma components. They approximate a multiple-peak velocity distribution with a multivariate Maxwellian mixture model where each component of the distribution represents one of the peaks. They suggested that the cold ions have their origin in the lobe, middle energy ions arise from an $\mathbf{E} \times \mathbf{B}$ drift, and the hot-ion component reflects an acceleration toward Earth. In a further analysis of this data by *Lui et al.* [2005], the authors found that the multicomponent values for the energy flux in the x-direction were typically larger by a factor of 2 from the single fluid approach while the values in the other directions were also quite different for the two approaches. These papers made no attempt to extract from their results a profile of the magnetic field across the current sheet to compare with the observed field.

[9] We have elected to model the separate identifiable ion groups as distinct fluid components. This is a significant step away from the single ion fluid assumption and toward a kinetic approach. The multifluid approach is particularly appropriate for the magnetotail current sheet where the asymptotic regions on opposite sides of the sheet can be regarded as independent sources of distinct plasmas. One fluid is the ions incoming from a source region far above the sheet. A second fluid is incoming from a source region far below the sheet. A third fluid describes massless electrons. With this model in mind, but now adopting a single particle viewpoint, Figure 1 illustrates trajectories (in scaled coordinates, see Table 1) for representatives from the first two of these groups in the deHoffman-Teller frame of reference [*de Hoffmann and Teller*, 1950], in which the cross-tail electric field vanishes ($E_y = 0$). We later (section 4) introduce the Earth reference frame but note that the deHoffman-Teller frame is moving in the x-direction (toward the Earth) with velocity E_y'/B_z, where E_y' is the y-component of the electric field in the Earth frame.

[10] Outside the sheet proper (roughly $|z| > 1$) the first two ion groups follow the magnetic field lines rather closely, except for their gyromotion. However, in the sheet itself (roughly $|z| < 1$ in the figure), they have much more irregular trajectories. The field lines themselves represent the trajectories of electrons, which, due to their small mass, have negligible gyromotion. The paths shown in Figure 1 are

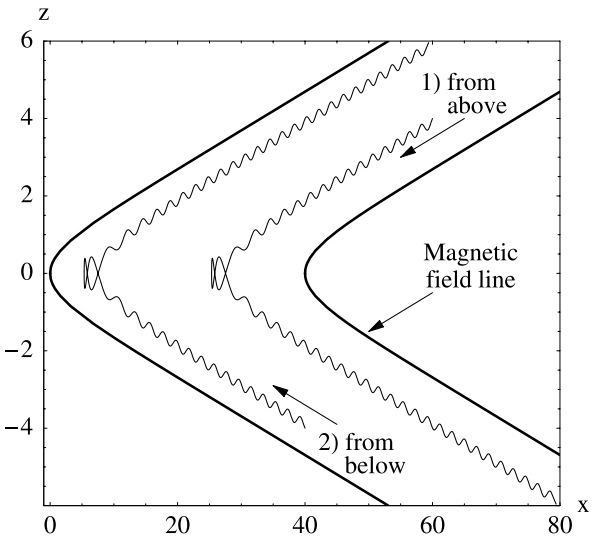

Figure 1. Ion trajectories in model magnetic field.

actually ion trajectories projected onto the (x, z) plane. Outside the sheet, ion y-motion is purely oscillatory, but in the sheet region, each ion trajectory makes a large, net excursion in the $+y$ direction (into the page). In the Earth's reference frame, there is an electric field component, $E'_y > 0$, which energizes ions undergoing these large excursions.

[11] In a truly collisionless plasma there are boundaries in velocity space between the three groups of ions. These boundaries can be quite complicated in general, but in the uniform-field regions outside the sheet, the velocity space boundary between groups 1 and 2 is simple, as illustrated in Figure 2.

[12] Not all group 1 and 2 ions behave exactly as shown in the figure. For example, some ions arriving from above, after negotiating the sheet, will travel back upward instead of crossing to the lower side. As such, an individual ion may jump from group 1 to group 2. This is a defect of the multifluid model as posed here. However, our focus is on the symmetric case (see section 4) where the asymptotic fields and particle sources on the upside and downside are identical. In this case, the possibility that some members of a group may change their identity is balanced by the fact that an equal number of members from the opposite group will do the same. Hence when comparing this multifluid theory with observations, one must carefully consider which phase space region comprises the domain of integration for a given component, before calculating fluid variables from a measured distribution function.

Table 1. Scaling Quantities for Dimensionless Variables[a]

Physical Quantity	Scale Value
Length (ion inertial length)	$L_{\rm ref} = c/\omega_{pi}$
Current density	$j_{\rm ref} = B_{\rm ref}/(\mu_0 L_{\rm ref})$
Velocity (Alfvèn speed)	$u_{\rm ref} = B_{\rm ref}/\sqrt{\mu_0 m_{\rm H} n_{\rm ref}}$
Pressure	$p_{\rm ref} = B^2_{\rm ref}/(2\mu_0)$
Temperature	$T_{\rm ref} = B^2_{\rm ref}/(2\mu_0 n_{\rm ref} k_B)$
Electric field	$E_{\rm ref} = B_{\rm ref} u_{\rm ref}$

[a]The ion plasma frequency is $\omega_{pi} = \sqrt{n_{\rm ref} e^2/(\epsilon_0 m_{\rm H})}$. As usual, ϵ_0 and μ_0 denote the permittivity and permeability of free space.

[13] A multifluid model has several advantages over a single fluid model. It retains more of the information present in a distribution function than a single fluid model captures. In particular, the single fluid model fails to correctly describe a plasma consisting of two streams. Another advantage is that our multifluid model extends in a natural way to include different ion species.

[14] We emphasize that our model is not an extension of the Harris kinetic model but rather a new fluid treatment. We define groups in terms of their source thereby making it possible to treat multiple sources emitting plasmas with different properties (e.g., possible different densities, temperatures, flows, and/or species). Groups with their own distinct flows means that the kinetic energy of each group is divided differently into drift and thermal components. The multiple fluid set of equations is derived by an integration of the Boltzmann/Vlasov system over different partial volumes of velocity space. It can be regarded as a step from fluid toward kinetic where the kinetic treatment in effect deals with an infinite number of groups, namely a distribution function with as many groups as there are distinct trajectories.

[15] In the model developed here, we assume that the remote asymptotic boundary conditions are known from measurements. This includes the normal field component, B_z, which is determined by remote current systems as mentioned earlier. Asymptotic properties of the incident fluid stream (pressure, density, flow speed) are assumed known since those particles originate from the remote region. The ejected fluid stream has interacted with the current sheet and been modified by it and thus no asymptotic boundary conditions are imposed on it. In the following calculations, we treat examples where the incoming groups have symmetric (and/or anti-symmetric) boundary conditions with the result that the ejected ion groups are related to the incoming groups by the equivalent symmetry conditions. However, we note that we deal mainly with the region where properties change significantly with z, and that

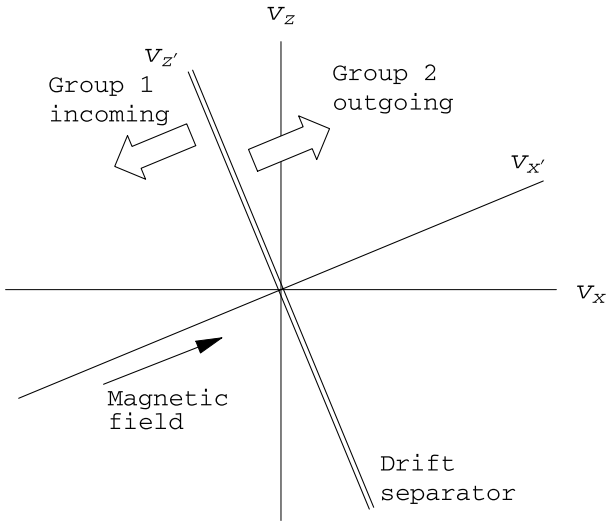

Figure 2. Groups 1 and 2 in velocity space far above the current sheet.

any position on the z-axis within that region could also be used for defining initial conditions.

3. Plasma-Field Equations for a One-Dimensional Multifluid

[16] Consider a collisionless, steady state plasma composed of multiple fluid groups: several ion fluid streams and a background of flowing electrons. These are treated as independent groups so that they interact with the electromagnetic field but not directly with each other. As such, the electromagnetic field organizes the various fluid streams so as to assure quasi-neutrality and consistency with magnetic field gradients (Ampere's law). Suppose also that the electrons are massless. Consistent with this is the assumption of quasi-neutrality and uniform electron temperature throughout the region, both in view of the high mobility of electrons along magnetic field lines.

[17] Restrict attention to the strictly one-dimensional geometry illustrated by the chevron-like field line structure in Figure 1 in which all variables depend only on the z (normal) coordinate. The possibility of an out-of-plane field component B_y is considered, but B_y vanishes in the symmetric case we consider in section 4.

[18] It is convenient to adopt a system of dimensionless variables based on only two basic scales: the reference magnetic field $B_{\rm ref}$ (chosen to be the asymptotic B_x for $|z| \gg 1$), and density $n_{\rm ref}$ (chosen to be the asymptotic value). Attention is limited to a hydrogen plasma so that the ion mass is $m_{\rm H}$ and the charge e. All other reference scales derive from these and are displayed in Table 1.

[19] In the weakly collisional regime relevant to space plasmas, the Chew-Golberger-Low (CGL) ion fluid model [*Chew et al.*, 1956] seems, at first, more realistic than a scalar pressure model (7). The CGL model allows for distinct parallel ($p_\parallel$) and perpendicular ($p_\perp$) ion pressures, which retain their separate identities because of the weak collisionality. For CGL fluids, the pressure gradient in the ion momentum equations would be replaced by $-\nabla \cdot \mathbf{\Pi}_\alpha$ with CGL stress tensor $\mathbf{\Pi}_\alpha = p_{\alpha\perp}(\mathbf{I} - \mathbf{bb}) + p_{\alpha\parallel}\mathbf{bb}$, where $\mathbf{b} = \mathbf{B}/B$ is a unit vector in the magnetic field direction. Here, and in what follows, the subscript α denotes the particular ion fluid group and subscript e denotes the electron fluid. The CGL model has two independent equations of state: $p_{\alpha\perp}/(n_\alpha B)$ = constant and $p_{\alpha\parallel}B^2/n_\alpha^3$ = constant. Unfortunately, the applicability of the CGL model requires that the magnetic field vary slowly on the ion gyroradius length scale. However, the typical current sheet thickness is comparable to the ion gyroradius. The result is a crosstalk between the perpendicular and parallel pressures in the sheet so that the two equations of state are not independent. Despite this obvious limitation, the CGL case was analyzed in the hope that it might lead to useful solutions. This enterprise failed. Integrating the equations leads to an unphysical result (negative values of $u_{\alpha y}^2$). This is most likely the consequence of the inapplicability of the anisotropic CGL equations of state in the current sheet region. In our model, two requirements for the use of CGL are violated near the center of the current sheet: the electric field is not perpendicular to the magnetic field, and there are important variations in pressure transport terms along magnetic field lines, [*Chew et al.*, 1956, p. 113, p. 117]. This difficulty does not affect the isotropic pressure model employed in this paper, which has no distinct parallel and perpendicular pressures. Further, the isotropic pressure led to no obviously unphysical results.

[20] The following equations are in the deHoffman-Teller frame unless stated otherwise. The conservation of fluid mass, $d(n_\alpha u_{\alpha z})/dz = 0$, and absence of magnetic monopoles, $dB_z/dz = 0$, integrate at once to give

$$u_{\alpha z} = \Gamma_\alpha/n_\alpha, \quad u_{ez} = \Gamma_e/n_e, \quad B_z = \text{const}, \tag{1}$$

where B_z, Γ_α, and Γ_e are constant parameters determined by the boundary conditions. Ampere's law connects the fields and the flow components:

$$\begin{aligned} \frac{dB_y}{dz} &= -\sum_\alpha n_\alpha u_{\alpha x} + n_e u_{ex} \\ \frac{dB_x}{dz} &= \sum_\alpha n_\alpha u_{\alpha y} - n_e u_{ey} \\ 0 &= \sum_\alpha n_\alpha u_{\alpha z} - n_e u_{ez}, \end{aligned} \tag{2}$$

where the sums are over all ion fluid groups. The quasi-neutrality assumption gives

$$n_e = \sum_\alpha n_\alpha. \tag{3}$$

[21] The three components of the ion momentum equation are

$$\Gamma_\alpha \frac{du_{\alpha x}}{dz} = n_\alpha u_{\alpha y} B_z - \Gamma_\alpha B_y \tag{4}$$

$$\Gamma_\alpha \frac{du_{\alpha y}}{dz} = \Gamma_\alpha B_x - n_\alpha u_{\alpha x} B_z \tag{5}$$

$$\Gamma_\alpha \frac{du_{\alpha z}}{dz} = -\frac{1}{2}\frac{dp_\alpha}{dz} - n_\alpha \frac{d\phi}{dz} + n_\alpha u_{\alpha x} B_y - n_\alpha u_{\alpha y} B_x, \tag{6}$$

where an electrostatic potential, ϕ, exists in view of the steady Faraday's law, $\nabla \times \mathbf{E} = 0$. The z-momentum equation employs a scalar pressure, which we assume is modeled by a polytropic law

$$p_\alpha = C_\alpha n_\alpha^\gamma, \tag{7}$$

where C_α is a constant and γ is the polytropic index ($\gamma = 5/3$ is assumed in the modeling that follows). The possibility of double-adiabatic ion groups was considered and discarded for reasons described earlier. Using (1b), the electron motion reduces simply to

$$\mathbf{u}_e = \Gamma_e \mathbf{B}/(n_e B_z). \tag{8}$$

[22] Using an electron thermal equation of state, $p_e(z) = n_e(z)\, T_e$ (dimensionless form), and because $\mathbf{u}_e \times \mathbf{B} = 0$, the electron z-momentum equation integrates to

$$\phi = (T_e/2) \log n_e, \tag{9}$$

the familiar Boltzmann relation.

[23] The system of equations can be simplified by eliminating the electron variables. Equations (7), (8), and (9), and quasi-neutrality, provide a way to write electron variables in terms of ion variables. Using these, Ampere's law and the z-component of the momentum equation become

$$dB_y/dz = \sum_\alpha \left(-n_\alpha u_{\alpha x} + \Gamma_\alpha B_x/B_z\right) \tag{10}$$

$$dB_x/dz = \sum_\alpha \left(n_\alpha u_{\alpha y} - \Gamma_\alpha B_y/B_z\right) \tag{11}$$

$$\Gamma_e = \sum_\alpha n_\alpha u_{\alpha z} = \sum_\alpha \Gamma_\alpha \tag{12}$$

$$\frac{d}{dz}\left(\frac{\Gamma_\alpha^2}{n_\alpha} + \frac{C_\alpha n_\alpha^\gamma}{2}\right) = n_\alpha\Big(u_{\alpha x}B_y - u_{\alpha y}B_x - \frac{T_e}{2}\sum_\alpha \frac{dn_\alpha}{dz}\Big/\sum_\alpha n_\alpha\Big) \tag{13}$$

[24] If there are N ion species, the complete system then amounts to a system of $3N + 2$ equations: N each of three momentum components (4), (5), and (13) and two from Ampere's law (10) and (11). The unknown dependent variables are B_x, B_y, and N each of n, u_x, and u_y. There are also $2N + 2$ constant parameters: Γ_α, C_α, B_z, and T_e.

4. Symmetric Three-Fluid System

[25] As an application of multifluid modeling, we now focus on the simplest example. Though the formalism can handle many and different types of fluids, (mass or charge state, equation of state), we examine a system of two passing ion fluids as illustrated in Figure 1. An assumption of symmetry, with respect to the sheet center $z = 0$, simplifies the model. Choose the two passing ion components to be identical except for their directions of motion ($u_{1x} = -u_{2x}$, $u_{1z} = -u_{2z}$, $u_{1y} = u_{2y} \equiv u_y$, $n_1 = n_2$). For a model current sheet, the x-components of magnetic field and flow speed are odd functions of z, whereas other variables are even functions.

[26] We have chosen to neglect trapped ions. *Francfort and Pellat* [1976] have shown that trapped ions are required for the existence of adiabatic solutions, where adiabatic refers to the preservation of the particle magnetic moment in transport through the current sheet. *Cowley and Pellat* [1979] showed how such solutions can be obtained for some specific particle velocity distributions. They also commented that solutions have been shown to exist without a trapped population but these are non-adiabatic and involve thin current layers. From a particle viewpoint, as opposed to a fluid model, trapped ions can exist in thin current sheets, and their first invariant is still preserved, but is described by a more complicated function than the magnetic moment in the thin sheet configuration, as mentioned in the introduction [*Schindler*, 1965; *Sonnerup*, 1971; *Whipple et al.*, 1986]. It is necessary to know the trapped particle velocity distribution at some point as an initial condition in order to find how the trapped particles mirror with position. This is beyond the scope of our present paper, which aims at dealing primarily with fluid properties, and so we only consider current sheet solutions which have no trapped particles. We believe that the multigroup approach provides greater flexibility of treatment in that the kinetic energy of each group involves both thermal and drift energy with the accompanying equations allowing interchange between these two forms of energy.

[27] The full model can now be represented on the half domain, $0 \le z < \infty$, with lower boundary at the sheet center, $z = 0$. At the asymptotic boundary, all variables must go smoothly to constants, that is, derivatives must vanish there. Also, by the symmetry conditions, we need only solve for one of the two passing components.

[28] Imposing the symmetry relations implies several features about the solutions and constants of integration. By our choice of reference quantities, the asymptotic tangential magnetic field is $B_x(\infty) = 1$. Because the normal ion fluxes are opposite, $\Gamma_1 = -\Gamma_2$. Then, the z-component of Ampere's law implies the electron fluid is motionless, $\mathbf{u}_e = 0$. In the asymptotic region, where derivatives vanish, the momentum equation implies the asymptotic ion flow is along the magnetic field line, $\mathbf{u}_1(\infty) \times \mathbf{B}(\infty) = 0$. It follows that $B_y = 0$ everywhere since: B_y is constant from (10); next apply (11) at infinity to find $u_{\alpha y}(\infty) = 0$; finally, apply (4) again at infinity to find $B_y = 0$. Because asymptotic ion density is $n_1(\infty) = 1/2$, the ion flow at infinity is $u_{1z}(\infty) = 2\Gamma_1$ and $u_{1x}(\infty) = 2\Gamma_1/B_z$.

[29] To anticipate physical interpretation, we replace constants in the equations of state and the Boltzmann relation (9) in terms of β, the ratio of fluid pressure to magnetic pressure. Using dimensional quantities, define constants $\beta_1 = 2\mu_0 p_1(\infty)/B_x^2(\infty)$ for an ion fluid, and $\beta_e = 2\mu_0 p_e(\infty)/B_x^2(\infty)$ for the electron fluid. Converting to dimensionless quantities (Table 1) and using equations of state for the two fluids, one finds

$$C_1 = C_2 = 2^\gamma \beta_1, \quad T_e = \beta_e. \tag{14}$$

[30] The equations developed in section 3 simplify under the assumption of symmetry as described in the next paragraphs. With the symmetry assumptions, the x-momentum equation for the passing ions (4) becomes

$$\frac{du_{1x}}{dz} = \frac{B_z n_1 u_y}{\Gamma_1} \tag{15}$$

[31] Eliminating $n_1 u_y$ between (11) and (15) leads to an exact integral

$$B_x - 2\Gamma_1 u_{1x}/B_z = \text{constant}, \tag{16}$$

for which the constant of integration vanishes in view of the odd symmetry for B_x and u_{1x} at the current sheet center. Evaluating (16) asymptotically, where $B_x(\infty) = 1$ and $u_{1x}(\infty) = 2\Gamma_1/B_z$, immediately yields

$$B_x = -u_{1x}, \quad 2\Gamma_1 = -B_z, \tag{17}$$

where we have made a choice of sign consistent with Figure 2. The three constant parameters, Γ_1, $u_{1z}(\infty) = \Gamma_1/n_1(\infty)$, and

B_z, are each fixed once one of them is chosen. An easy result from (17) is that the asymptotic tangential flow velocity is at the asymptotic Alfvèn speed, that is, $u_{1x}(\infty) = -1$.

[32] Now replace u_{1x} with B_x in the momentum conservation equations (15), (5), and (13) to find

$$\frac{dB_x}{dz} = 2n_1 u_y \tag{18}$$

$$\frac{du_y}{dz} = B_x(1 - 2n_1) \tag{19}$$

$$\frac{d}{dz}\left(\frac{B_z^2}{4n_1} + \frac{\beta_1(2n_1)^\gamma}{2}\right) = -\frac{B_x}{2}\frac{dB_x}{dz} - \frac{\beta_e}{2}\frac{dn_1}{dz}. \tag{20}$$

[33] Thus (18), (19), and (20) are explicit differential equations for B_x, u_y, and n_1. These equations contain three dimensionless parameters, β_e, β_1, and B_z.

[34] Because the independent variable, z, does not appear explicitly in the differential equations, one can convert the differential equations into quadratures. Introducing a combined ion density $n = n_1 + n_2 = 2n_1$ and $\beta_i = \beta_1 + \beta_2 = 2\beta_1$, we integrate (20) and replace d/dz with $(dn/dz)\, d/dn$ in (18) and (19) to find

$$B_x^2 = 1 + \beta_i(1 - n^\gamma) + \beta_e(1 - n) + 2B_z^2(1 - 1/n) \tag{21}$$

$$u_y^2 = -B_z^2\left(1 - \frac{1}{n}\right)^2 + \beta_i\left(\frac{\gamma(1 - n^{\gamma-1})}{\gamma - 1} + n^\gamma - 1\right) + \beta_e(n - 1 - \log n), \tag{22}$$

valid when $\gamma \neq 1$, and for which constants of integration were evaluated by using the boundary conditions at infinity. The $\gamma = 1$ case is also straightforward to evaluate.

[35] Algebraic expressions (21) and (22) have several practical applications. One is that they provide a convenient method to estimate density and out-of-plane flow (u_y) in the center region using parameters and conditions measured in the asymptotic region. For instance, using $B_x(0) = 0$ in (21) gives an algebraic equation for the central current sheet density. Once that density is known, (22) immediately gives the out-of-plane flow speed at the center.

[36] As a second example of usefulness, consider a satellite pass through a 1-D quiet current sheet, for which distances to the center ($z = 0$) are not accurately known. Even so, (21) and (22) provide specific predictions of the relations between measured variables, such as magnetic field, flow velocity, and density. Compare (21) with the less versatile dimensionless Harris model relation between magnetic field and density, $B_x^2(z)/B_x^2(\infty) = 1 - n(z)/n(0)$.

[37] A third way in which (21) and (22) are useful is that they offer insight upon conditions which will ensure physically realistic solutions from the mathematical model. Specifically, the left hand side of (22) is non-negative. Hence the right hand side of (22) is non-negative, and there is a relationship between physical non-negative parameters B_z^2, β_e, and β_i. For instance, if β_e and β_i are sufficiently small and $n \neq 1$, the first term on the right side of (22) dominates and there is no physical solution. Thus the equations imply constraints on the values of the model parameters.

[38] The former analysis also works nicely when choosing the center region as a base, in place of the asymptotic region. This alternate formulation is useful for data analysis. The current sheet center is a specific location, identified by the direction change in magnetic field, while the asymptotic region is less precisely defined. Hence it is advantageous to formulate model results in terms of parameters and reference quantities based on their measured values in the central region. The center density, $n_e(0) = n(0)$ is a convenient reference density. Because B_x vanishes at the sheet center, it cannot be used for the magnetic field scale. Instead, choose B_z as the reference magnetic field. With these choices, parameters β_{e0} and β_{i0} (total ion beta) are computed as the ratio of central current sheet fluid pressures to magnetic $(B_z^2/(2\mu_0))$ pressure. With B_z as the reference field, its value is no longer available as a model parameter. For the third model parameter, the ratio $M \equiv u_{1z}(0)\sqrt{m_{\mathrm{H}} n(0)\mu_0}/B_z$, an Alfvèn Mach number in the central current sheet, is a convenient choice. Using a normalization with respect to sheet center quantities and the new parameters $\{M, \beta_{e0}, \beta_{i0}\}$, the relation between B_x and u_{1x} is $B_x = -u_{1x}M^2$ instead of (17). Combining this with $\mathbf{u}_1 \times \mathbf{B} = 0$ and the constancy of $n_1\, u_{1z}$, one finds the asymptotic density is simply $n(\infty)/n(0) = M^2$. A measure of one ion component's normal flow, density, and the normal magnetic field at the sheet center predicts the asymptotic density through this simple relation. As another example, when normalized by central values, equation (21) becomes

$$B_x^2 = 2M^2(1 - 1/n) + \beta_{i0}(1 - n^\gamma) + \beta_{e0}(1 - n) \tag{23}$$

Using the asymptotic density, we impose the physical constraint $B_x^2(M^2) > 0$ which translates to a condition on the parameters in (23): if $M < 1$, $\beta_{e0} \geq 2 - \beta_{i0}(1 - M^{2\gamma})/(1 - M^2)$. This restriction is a necessary condition for a physical solution, but not a sufficient condition. It is possible that solutions may be physically unrealistic for reasons not yet considered.

[39] All the foregoing equations are in the deHoffman-Teller frame where $E_y = 0$. In the remainder of this section, we use non-normalized MKS units to connect the model with measurements made from another reference frame. (We mark quantities with different values in this new reference frame with a prime.) Let us transform to a satellite frame (close to Earth's frame), in which an electric field $E_y' > 0$ is measured. In that case, the tangential velocity shift is $V_x = -E_y'/B_z < 0$. For illustration, measurements of the fluid velocity toward the Earth range from 0–600 km/s [*Baumjohann et al.*, 1988]. Baumjohann also noted that high-speed flows are field-aligned and directed toward the Earth.

[40] Finally, consider the Poynting flux $\mathbf{S}' = (\mathbf{E}' \times \mathbf{B})/\mu_0$ in the Earth frame, which describes the flux of the field energy. This has three components, one in the x-direction, $S_x' = E_y' B_z/\mu_0$, which is independent of position. The y-component is $S_y' = E_z B_x/\mu_0$ where E_z comes from the electric potential required for quasi-neutrality, equation (3). Component S_y' varies with position through $B_x(z)$, but this change does not contribute to the divergence of $\mathbf{S}'$. The

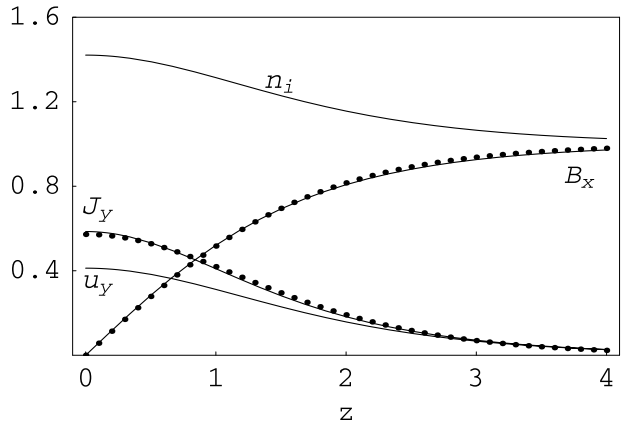

Figure 3. Magnetic field, current density, ion density and out-of-plane flow for $B_z = 0.1$, $\beta_e = 0.5$, $\beta_i = 1$. Solid lines are fluid model results and dot symbols are from the Harris sheet solution.

z-component, $S_z' = -E_y' B_x/\mu_0$, also varies with z, changing from positive to negative in crossing the $z = 0$ plane from below to above. Considering its sign, S_z' describes the flux of electromagnetic energy traveling toward the center from both sides. Approaching the central sheet, the divergence of the Poynting flux is negative, implying the conversion of electromagnetic energy into fluid energy. This is confirmed by comparing the change in electromagnetic energy density, $\nabla \cdot \mathbf{S}'$, with the change in fluid energy density, $\mathbf{E}' \cdot \mathbf{J}$:

$$\nabla \cdot \mathbf{S}' = dS_z'/dz = -d\left(E_y' B_x/\mu_0\right)/dz$$
$$= -\left(E_y'/\mu_0\right) dB_x/dz = -E_y' J_y = -\mathbf{E}' \cdot \mathbf{J}. \quad (24)$$

Since $\nabla \cdot \mathbf{S}' + \mathbf{E}' \cdot \mathbf{J} = 0$, energy is conserved as electromagnetic energy is transformed into fluid kinetic energy during the fluid crossing of the central region and acceleration by the electric field. This acceleration of ions as they cross the $z = 0$ plane from both directions has been recognized and discussed previously [*Eastwood*, 1972; *Hill*, 1975; *Lyons and Speiser*, 1982; *Whipple et al.*, 1990] but has not been emphasized in many treatments of plasma behavior in the magnetotail, perhaps because the appearance of this transformation of energy depends on the reference frame and does not occur in the deHoffman-Teller frame where $E_y = 0$.

5. Computational Results

[41] The multifluid model developed in sections 3 and 4 (deHoffman-Teller reference frame) is used here to study a specific example and the effects of model parameters. Some important output quantities from this exercise include: (1) sheet thickness, the half-thickness δ is defined in Appendix A; (2) density peaking, the ratio of density at the sheet center to the asymptotic value $n(0)/n(\infty)$; (3) current density and magnetic field profiles, which we compare with the familiar Harris solution using the same δ, $B_x = \tanh(z/\delta)$ and $j_y = \mathrm{sech}^2(z/\delta)/\delta$.

[42] Figure 3 shows the magnetic field, current density, ion density and out-of-plane flow calculated from the model with parameters $B_z = 0.1$, $\beta_e = 0.5$, and $\beta_i = 1$. The model (solid curves) is close to the scaled Harris profile (dots) even for the more sensitive current density profile. For this example, the computed sheet thickness is $\delta = 1.748$ and the ratio of central to asymptotic density is $n(0)/n(\infty) = 1.42$. Unlike Harris' solution, the out-of-plane flow speed is not uniform and the density does not fall to zero asymptotically. The resemblance in B_x for these two different models arises in part because the fluid model assumes the same asymptotic and symmetry properties that Harris found, because similar equations are used, and because the hyperbolic tangent model is scaled to match the fluid model at an intermediate point. The resemblance might also be explained in terms of the finding of *Lui et al.* [1995] that a simple pressure relation together with a broad profile of u_y with z tends toward the Harris current sheet.

[43] The usefulness of a current sheet model depends on its predictive nature. Here we examine several important sheet properties and trends that emerge from the model. In particular consider the dependence of two quantities, shown in Figure 4, on the asymptotic ion pressure (expressed as β_i). The first quantity, δ, is the current sheet thickness (in units of c/ω_{pi}). The second quantity, $n(0)/n(\infty)$, is the density peaking, center-to-asymptotic. While these examples assume $B_z = 0.1$, the cases $B_z = 0.05$, 0.2 almost exactly overlay the curves shown.

[44] Several specific predictions arise from the symmetric model.

5.1. Asymptotic Tangential-Drift

[45] In the asymptotic region, comparing (17), the flow of each fluid component is field-aligned at the Alfvèn speed. In particular, the two fluid components have a velocity difference of twice the Alfvèn speed measured in any inertial reference frame. Because the model assumes no time dependence, we have not investigated the stability of this configuration of crossing ion beams. To transform a calculated u_{1x} from the model frame (unprimed) to a new frame (primed), one should use the transformation velocity $V_x = -E_y'/B_z$, where E_y' is the electric field in the new frame. That is, the relation between measured (new) and model (deHoffman-Teller) flows is $u_{1x}' = u_{1x} - V_x = u_{1x} + E_y'/B_z$.

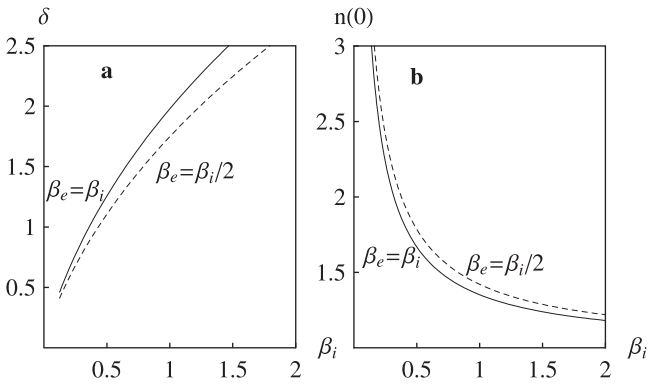

Figure 4. Dependence of sheet parameters on ion pressure: $B_z = 0.1$; $\beta_e/\beta_i = 1$, 0.5.

5.2. Current Sheet Thickness

[46] According to Figure 4a the current sheet thickness is related to the asymptotic ion pressure parameter β_i. The dependence on B_z is weak enough that the curves essentially overlay. The model results suggest that the magnitude of B_z has little effect on the sheet thickness. There is only a modest dependence on the electron-to-ion pressure ratio β_e/β_i. From Figure 4a, the approximate relationship between the current sheet thickness and the ion pressure parameter is

$$\delta \approx 2\sqrt{\beta_i}. \tag{25}$$

[47] Thus higher ion pressure at infinity is associated with a broadened sheet. Also shown is the cool electron case $\beta_e/\beta_i = 1/2$. Evidently cooler electrons reduce the sheet thickness slightly but the effect is somewhat weaker than the ion pressure (β_i) effect.

5.3. Density Peaking

[48] According to Figure 4b, the ratio of the sheet-center density to the asymptotic density is also related to the ion pressure parameter. The curves in Figure 4b show an approximate dependence

$$n(0)/n(\infty) \approx 1 + 1/(3\beta_i). \tag{26}$$

Thus higher ion pressure in the asymptotic region is associated with decreased density peaking. Also shown is the cooler electron case: cooler electrons far from the current sheet reduce the total pressure and thus tend toward more peaked density, the same as lower ion pressure. Again the electron pressure is less important than the ion pressure. In terms of asymptotic parameters, $\{B_z,\ \beta_i,\ \beta_e\}$, (26) approximates the ratio of central to asymptotic densities. A different choice of parameters, that is, a transformation to new coordinates in parameter space, can lead to a simpler relation between parameters and the density ratio. Using the parameter set, $\{M, \beta_{e0}, \beta_{i0}\}$, the relation is $n(0)/n(\infty) = 1/M^2$. That is, the density peaking depends only on the Alfvèn Mach number of the normal flow at the current sheet center, and not on the β's at the center, such that slower flow is associated with a higher density ratio (smaller asymptotic density).

5.4. Magnetic Field Profile

[49] The Harris model predicts a specific form of the (tangential) magnetic field. In dimensionless units, this result is $B_x^2 = 1 - n$, in which the reference field is the asymptotic value and the reference density is the center ($z = 0$) value. The symmetric multifluid model result (21) predicts that B_x^2 varies with density as n, n^γ, and $1/n$, where the coefficients depend upon β for the ion and electron fluids, and B_z. Thus the multifluid model describes a broader range of plasma and magnetic field configurations than the Harris model does.

6. Comparison of Multifluid Model and Measurements

[50] A number of quantities can be taken directly from satellite measurements of electric and magnetic fields and their structure, e.g., $B_x(\infty)$, B_z, E_y', δ, or inferred by taking moments of the measured distribution, e.g., $n_1(0)$, $n_1(\infty)$, $u_{1x}(\infty)$, T_1, or T_e. The model predicts several simple relationships between these quantities that can readily be checked. In this section, we illustrate these relations, using dimensional quantities, through the use a hypothetical two component Maxwellian distribution function (see Appendix B) as a proxy for a measured distribution function which might be obtained in the Earth (satellite) reference frame. If such measurements are to provide boundary conditions or other constraints for a model calculation, then some of them may need to be transformed into the deHoffmann-Teller frame using $V_x = +E_y'/B_z$, which is the inverse of the transformation discussed in section 4.

6.1. Asymptotic Tangential-Drift

[51] From the discussion following (17), the tangential jump that an ion stream experiences after negotiating the current sheet is $\Delta u_{1x}(\infty) = 2|u_{1x}(\infty)| = 2$. Restoring the dimensional variables to this gives,

$$\Delta u_{1x}(\infty) = 2B_x(\infty)/\sqrt{\mu_0 m_H n(\infty)}. \tag{27}$$

This equation is consistent with the single particle relation, in Earth's reference frame, $v_{xf} = 2E_y'/B_z - v_{xi}$, which relates the final speed ($v_{xf} > 0$) of an ion, after traversing the current sheet, to its initial speed ($v_{xi} < 0$) [*Hill*, 1975; *Whipple et al.*, 1990]. The relation follows from the constancy of the first adiabatic invariant, which, unlike the magnetic moment, is preserved through the central region. Because the invariant reverts to the magnetic moment far from the current sheet, the initial perpendicular kinetic energy is recovered, and the energy that was gained in the Earth frame appears as higher field-aligned velocity. Because $E_y = 0$ in the deHoffman-Teller frame, $\Delta v_x \equiv v_{xf} - v_{xi} = -2v_{xi}$ is the change in tangential velocity for a single ion, consistent with the ion fluid component change (27). Appendix B provides an example of computing the fluid drift speed (u_{1x}) from a measured distribution function.

6.2. Current Sheet Thickness

[52] The current sheet thickness scales with the square root of the asymptotic total ion β_i (25). For a structured distribution function, the parameter $\beta_1 \equiv (2p_1\mu_0/B_x^2)|_\infty)$ should utilize the perpendicular pressure or temperature since these parameters are the same for both groups 1 and 2, and do not also involve the relative motion of the two groups (B7). In contrast, the parallel pressure and temperature do depend upon the drift and thermal energies (B6). Using the relation between temperature and pressure for the two component Maxwellian distribution, the current sheet thickness can be written as

$$\delta = \sqrt{8}\rho_i(\infty) \tag{28}$$

where $\rho_i(\infty) \equiv \sqrt{m_H k_B T_{i\perp}}/(eB_x(\infty))$ is the asymptotic ion gyroradius. Interestingly, although the central ion inertial length c/ω_{pi} is the conventional length scale for the current sheet, the model predicts also that the current sheet thickness is proportional to the asymptotic ion gyroradius. Thus (28) is a prediction of a relationship between the quantities δ, B_x, and $T_\perp$.

6.3. Density Peaking

[53] Re-introduce dimensional quantities in (26):

$$3\left(\frac{n(0)}{n(\infty)}-1\right)=\frac{B_x^2(\infty)}{2\mu_0 n(\infty)k_B T_{i\perp}}. \tag{29}$$

This is a prediction of a relationship between $n(0)$, $n(\infty)$, $T_i(\infty)$, and $B_x(\infty)$.

7. Summary

[54] In summary, the multigroup ion model is an improvement on the Harris model in that a normal magnetic field is included; it allows the presence of counterstreaming components, a non-zero asymptotic density, and an out-of-plane drift speed that vanishes far from the sheet center. Further, it gives rise to predictive relationships between the ion pressure, the current sheet thickness, and the density peaking factor. The fluid equations are relatively simple and can be easily handled numerically. This work is preliminary in that we have not yet attempted to calculate the results for asymmetric boundary conditions for the fields and plasma properties. However, the separation into groups allows the assignment of different initial properties, subject to the requirement for pressure balance across the sheet.

[55] We have found that the simple CGL equation of state (anisotropic pressure of the ion groups) yields no solutions, at least in the symmetric case. It would be useful if new equations of state with anisotropic pressures could be derived based on the magnetotail configuration with a large magnetic field gradient in the sheet region. Such equations would have to allow for the resulting non-collisional cross-talk between the parallel and perpendicular pressures.

[56] Comparison of satellite data in the region of the central plasma sheet with a theoretical calculation of its structure is complicated by the necessity of finding the reference frame that is appropriate to use for the local geometry of the sheet itself. This problem has been discussed in detail by a number of authors, notably by Tsyganenko and his collaborators [*Tsyganenko et al.*, 1998; *Tsyganenko*, 1998; *Tsyganenko and Fairfield*, 2004].

[57] As a simple first description viewed in Earth's reference frame, plasma accelerated toward the Earth suggests a plasma source deep in the magnetotail. However, the multifluid model demonstrates a plausible alternate description. Before acceleration, this plasma comes from regions closer to the Earth, and, while crossing the current sheet, is turned back toward the Earth by the acceleration process. Thus there is no need for a deep-tail plasma source. The ion energy gain comes from the loss of electromagnetic energy as described by the Poynting flux. Further, this process exists independently of the B_x profile, at least for the present example of an isotropic plasma and monotonic $B_x(z)$.

[58] We have shown that multigroup models provide a manageable means for fluid theories to incorporate effects arising from distribution functions that are more structured than a Maxwellian. This is important because structured distribution functions are commonly observed near Earth's magnetotail current sheet, and their incorporation into models should improve the quality of current sheet descriptions. The model's analytic simplicity was purchased by making several approximating assumptions, including a one-dimensional structure, no time dependence, and simple equations of state for ions and electrons. Future efforts will compare such models to current sheet measurements, with the following goals: learning which current sheet features are not correctly modeled, identifying more appropriate equations of state, and investigating the role of electrons in current sheet structure.

Appendix A: Definition of Sheet Thickness

[59] Define the (dimensionless) sheet thickness, δ, as follows:

$$\delta=\frac{B_x^{-1}(1-1/e)}{\tanh^{-1}(1-1/e)}\approx 1.34B_x^{-1}(0.632) \tag{A1}$$

What this means is that one first locates the z value at which the tangential magnetic field is about 63% of its maximum. This value is then scaled by the location where a hyperbolic tangent magnetic field profile would reach the same 63% of maximum level. The hyperbolic tangent form is used to facilitate comparison with the Harris current sheet. For example, a profile rising to its maximum value faster than a Harris model has $\delta < 1$, that is a decreased thickness parameter. This method of determining thickness is better than the simpler $\delta = 1/(dB_x(0)/dz)$ because the simpler definition gives a misleading large sheet thickness in the case of a hollow current profile, for which dB_x/dz is very small at the sheet center. (Multiply δ by the length scale—asymptotic ion inertial length—to obtain a dimensional thickness.)

Appendix B: Connection Between Kinetic and Fluid Pictures of the Ions

[60] In the deHoffman-Teller frame of reference, consider a two component Maxwellian distribution representing the overall distribution of ions at points in the asymptotic region above the current sheet ($z > 0$).

$$f(\mathbf{v})=\frac{n_0}{2\pi^{3/2}v_t^3}\left(\exp\left(-\frac{(v_{x'}+V_d)^2+v_y^2+v_{z'}^2}{v_t^2}\right)+\exp\left(-\frac{(v_{x'}-V_d)^2+v_y^2+v_{z'}^2}{v_t^2}\right)\right) \tag{B1}$$

where n_0, v_t, and V_d are constants. Figure B1 shows contours of constant f for this distribution in which the $v_{x'}(v_{z'})$ coordinate is aligned with (perpendicular to) the asymptotic magnetic field. The two terms in (B1) comprise an approximate simple model for the two ion fluids we have introduced in section 4. The first (second) term in (B1) includes nearly all the ions incoming (outgoing), and is therefore roughly the same as group 1 (group 2). This identification of terms is imperfect in that some of the ions described by the first term are outgoing, and therefore belong in group 2. The drift speeds associated with the two terms in (B1), $-V_d$ for the first and $+V_d$ for the second term, approximate the flow speeds of the two fluid components, group 1 and group 2.

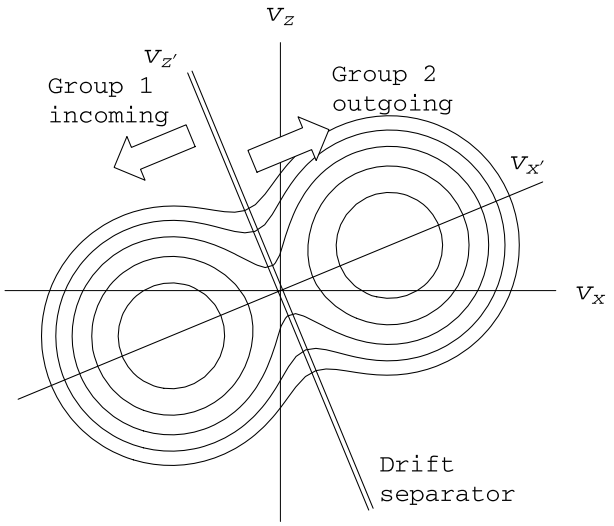

Figure B1. Two component Maxwellian distribution at an observation point above the current sheet.

[61] More precisely, the group 1 and group 2 fluid components are separated by the drift-separator surface $v_{x'} = 0$ (see Figure B1). The ranges in velocity space occupied by the two groups are:

$$\text{Group 1}: -\infty < v_{x'} < 0 \quad -\infty < v_y, v_{z'} < +\infty \tag{B2}$$

$$\text{Group 2}: 0 < v_{x'} < +\infty \quad -\infty < v_y, v_{z'} < +\infty. \tag{B3}$$

Computing the moments of the distribution function for the two groups requires a careful determination of the proper ranges of integration in velocity space. The relevant moments of the distribution function for the group 1 and 2 fluids are

$$n_1 = n_2 = n_0/2 \tag{B4}$$

$$\langle v_{x'} \rangle_1 = -\langle v_{x'} \rangle_2 = -v_t \left(\frac{e^{-(V_d/v_t)^2}}{\sqrt{\pi}} + \frac{V_d}{v_t} \mathrm{erf}\left(\frac{V_d}{v_t} \right) \right) \tag{B5}$$

$$T_{\|1} = T_{\|2} = \frac{m_\mathrm{H} v_t^2}{4k_B} \left(1 + 2V_d^2/v_t^2 + 2\left(\frac{e^{-(V_d/v_t)^2}}{\sqrt{\pi}} + \frac{V_d}{v_t} \mathrm{erf}\left(\frac{V_d}{v_t} \right) \right)^2 \right) \tag{B6}$$

$$T_{\perp 1} = T_{\perp 2} = \frac{m_\mathrm{H} v_t^2}{4k_B}. \tag{B7}$$

[62] Note that the temperature of the two groups is anisotropic to some degree, although the anisotropy decreases ($T_\perp/T_\| - 1 \to 0$) for increasing V_d/v_t.

[63] An alternative to the two component Maxwellian model (B1) is the usual (single) Maxwellian distribution, as illustrated in Figure B2. This is the $V_d/v_t \to 0$ limit of the two component Maxwellian. We view the usual isotropic Maxwellian distribution as the union of an incoming and outgoing component, separated by the $v_{x'} = 0$ plane. In this viewpoint, although their union is an isotropic equilibrium distribution, each of the groups is highly anisotropic. For instance, $T_{\|1} = (1-2/\pi)T_{\perp 1} = 0.36T_{\perp 1}$ from the limit $V_d/v_t \to 0$ in (B6). By contrast, the individual groups in the two component Maxwellian are nearly isotropic, especially as $V_d \gg v_t$. On the other hand, the Maxwellian distribution is the only example in the magnetotail that has been analyzed in detail [*Lyons and Speiser*, 1982].

[64] While the individual groups in the two component Maxwellian model are isotropic, the overall bulk distribution combining the two ion groups is not. The moments of the full distribution differ from those shown in (B5)–(B7). Thus for example, the mean velocity of the combined ion groups, in the asymptotic region as viewed from Earth's reference frame, is E_y'/B_z. (There is also a mean drift of the combined ion groups close to the current sheet in the y direction.) The temperature anisotropy of the combined groups is likely to be considerable:

$$\frac{T_{\perp,\mathrm{bulk}}}{T_{\|,\mathrm{bulk}}} - 1 = -\frac{2V_d^2}{v_t^2 + 2V_d^2} \tag{B8}$$

From this, one can find the field-aligned drift speed of the two Maxwellian components in (B1), in terms of the combined ion population's moments, as computed from the measurements:

$$V_d = \sqrt{2k_B\left(T_{\|,\mathrm{bulk}} - T_{\perp,\mathrm{bulk}}\right)/m_H} \tag{B9}$$

[65] One could extend this analysis by inserting expressions for V_d and v_t (in terms of $T_{\perp,\mathrm{bulk}}$ and $T_{\|,\mathrm{bulk}}$) into (B5), to obtain $\langle v_{x'} \rangle$ in terms of the bulk distribution's moments. The derived expression would be limited in application to a distribution function consisting of two identical Maxwellian components. Nevertheless, this exercise demonstrates the

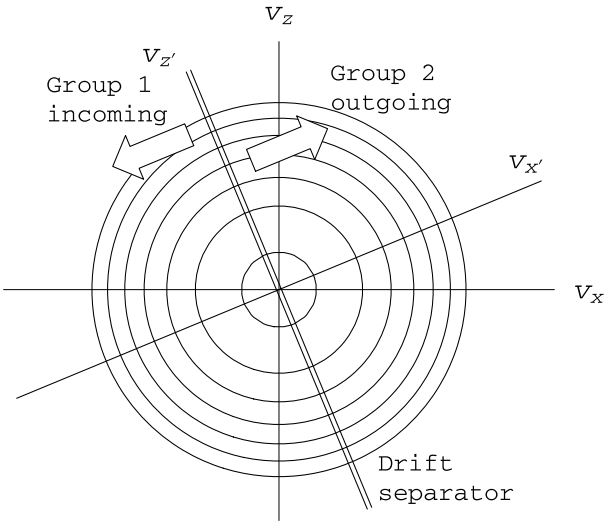

Figure B2. Single component Maxwellian distribution at an observation point above the current sheet.

process of obtaining the required multifluid quantities from observed distribution functions.

[66] **Acknowledgments.** This work was supported by NASA under the Cluster mission by grants NAG5-4686 and NNG04GF23G to the University of Washington and grant NAG5-6935 to the University of New Hampshire.

[67] Amitava Bhattacharjee thanks the reviewers for their assistance in evaluating this paper.

References

Asano, Y., et al. (2005), How typical are atypical current sheets?, *Geophys. Res. Lett.*, *32*, L03108, doi:10.1029/2004GL021834.

Baumjohann, W. (1998), Ion and electron heating in the near-earth magnetotail, in *New Persectives on the Earth's Magnetotail*, edited by A. Nishida, D. N. Baker, and S. W. H. Cowley, AGU Geophysical Monograph 105.

Baumjohann, W., G. Paschmann, N. Sckopke, C. A. Cattell, and C. W. Carlson (1988), Average ion moments in the plasma sheet boundary layer, *J. Geophys. Res.*, *93*, 11,507.

Baumjohann, W., G. Paschmann, and C. A. Cattell (1989), Average plasma properties in the central plasma sheet, *J. Geophys. Res.*, *94*(A6), 6597.

Chew, G. F., M. L. Goldberger, and F. E. Low (1956), The Boltzmann equation and the one-fluid hydromagnetic equations in the absence of particle collisions, *Proc. R. Soc., Ser. A and Ser. B*, *A236*, 112.

Cowley, S. W. H. (1978a), A note on the motion of charged particles in one-dimensional magnetic current sheets, *Planet. Space Sci.*, *26*, 539.

Cowley, S. W. H. (1978b), The effect of pressure anisotropy on the equilibrium structure of magnetic current sheets, *Planet. Space Sci.*, *26*, 1037.

Cowley, S. W. H., and R. Pellat (1979), A note on adiabatic solutions of the one-dimensional current sheet problem, *Planet. Space Sci.*, *27*, 265.

de Hoffmann, F., and E. Teller (1950), Magneto-hydrodynamic shocks, *Phys. Rev.*, *80*(4), 692.

Eastwood, J. W. (1972), Consistency of fields and particle motion in the ''Speiser'' model of the current sheet, *Planet. Space Sci.*, *20*, 1555.

Francfort, P., and R. Pellat (1976), Magnetic merging in collisionless plasmas, *Geophys. Res. Lett.*, *3*, 433.

Harris, E. G. (1962), On a plasma sheath separating regions of oppositely directed magnetic field, *Il Nuovo Cimento*, *23*, 115.

Hill, T. W. (1975), Magnetic merging in a collisionless plasma, *J. Geophys. Res.*, *80*, 4689.

Kan, J. R. (1973), On the structure of the magnetotail current sheet, *J. Geophys. Res.*, *78*, 3773.

Lui, A. T. Y. (2004), Potential plasma instabilities for substorm expansion onsets, *Space Sci. Rev.*, *113*, 127.

Lui, A. T. Y., C. L. Chang, and P. H. Yoon (1995), Preliminary nonlocal analysis of cross-field current instability for substorm expansion onset, *J. Geophys. Res.*, *100*, 19,147.

Lui, A. T. Y., T. Hori, G. Ueno, and T. Mukai (2005), Plasma transport from multicomponent approach, *Geophys. Res. Lett.*, *32*, L06101, doi:10.1029/2004GL021891.

Lyons, L. R. (1984), Electron energization in the geomagnetic tail current sheet, *J. Geophys. Res.*, *89*, 5479.

Lyons, L. R., and T. W. Speiser (1982), Evidence for current sheet acceleration in the geomagnetic tail, *J. Geophys. Res.*, *87*, 2276.

Parks, G. K. (2004), Why space physics needs to go beyond the MHD box, *Space Sci. Rev.*, *113*, 91.

Parks, G. K., L. J. Chen, M. Fillingim, R. P. Lin, and M. McCarthy (2001), Kinetic characterization of plasma sheet dynamics, *Space Sci. Rev.*, *95*, 237.

Schindler, K. (1965), Adiabatic particle orbits in discontinuous fields, *J. Math. Phys.*, *6*, 3313.

Schindler, K., (1972), A self-consistent theory of the tail of the magnetosphere, in *Earth's Magnetospheric Processes*, edited by B. M. McCormac, p. 200, D. Reidel Pub. Co., Dordrecht-Holland.

Schindler, K. (1975), Plasma and fields in the magnetospheric tail, *Space Sci. Rev.*, *17*, 589.

Schindler, K. (1979), Theories of tail structures, *Space Sci. Rev.*, *23*, 365.

Sestero, A. (1966), Vlasov equation study of plasma motion across magnetic fields, *Phys. Fluids*, *9*, 2006.

Sitnov, M. I. (2006), Structure and dynamics of a new class of thin current sheets, *J. Geophys. Res.*, *111*, A08204, doi:10.1029/2005JA011517.

Sonnerup, B. U. O. (1969), Acceleration of particles reflected at a shock front, *J. Geophys. Res.*, *74*, 1301.

Sonnerup, B. U. O. (1971), Adiabatic particle orbits in a magnetic null sheet, *J. Geophys. Res.*, *76*, 8211.

Speiser, T. W. (1965a), Particle trajectories in a model current sheet, based on the open model of the magnetosphere, with applications to auroral particles, *J. Geophys. Res.*, *70*, 1717.

Speiser, T. W. (1965b), Particle trajectories in model current sheets, 1, Analytical solutions, *J. Geophys. Res.*, *70*, 4219.

Speiser, T. W. (1967), Particle trajectories in model current sheets, 2, Applications to auroras using a geomagnetic tail model, *J. Geophys. Res.*, *72*, 3919.

Speiser, T. W. (1970), Conductivity without collisions or noise, *Planet. Space Sci.*, *18*, 613.

Thompson, S. M., M. G. Kivelson, M. El-Aloui, A. Balogh, H. Reme, and L. M. Kistler (2006), Bifurcated current sheets: Statistics from Cluster magnetometer measurements, *J. Geophys. Res.*, *111*, A03212, doi:10.1029/2005JA011009.

Tsyganenko, N. A. (1995), Modeling the earth's magnetospheric magnetic field confined within a realistic magnetopause, *J. Geophys. Res.*, *100*, 5599.

Tsyganenko, N. A. (1998), Modeling of twisted/warped magnetospheric configurations using the general deformation method, *J. Geophys. Res.*, *103*(23), 551.

Tsyganenko, N. A., and D. H. Fairfield (2004), Global shape of the magnetotail current sheet as derived from Geotail and Polar data, *J. Geophys. Res.*, *109*, A03218, doi:10.1029/2003JA010062.

Tsyganenko, N. A., and T. Mukai (2003), Tail plasma sheet models derived from Geotail particle data, *J. Geophys. Res.*, *108*(A3), 1136, doi:10.1029/2002JA009707.

Tsyganenko, N. A., S. B. P. Karlsson, S. Kokubun, T. Yamamoto, A. J. Lazarus, K. W. Ogilvie, C. T. Russell, and J. A. Slavin (1998), Global configuration of the magnetotail current sheet as derived from Geotail, Wind, IMP 8 and ISEE 1/2 data, *J. Geophys. Res.*, *103*, 6827.

Ueno, G., N. Nakamura, T. Higuchi, T. Tsuchiya, S. Machida, T. Araki, Y. Saito, and T. Mukai (2001), Application of multivariate Maxwellian mixture model to plasma velocity distribution function, *J. Geophys. Res.*, *106*, 25,655.

Whipple, E. C., T. G. Northrop, and T. J. Birmingham (1986), Adiabatic theory in regions of strong field gradients, *J. Geophys. Res.*, *91*, 4149.

Whipple, E. C., M. Rosenberg, and M. Brittnacher (1990), Magnetotail acceleration using generalized drift theory: A kinetic merging scenario, *Geophys. Res. Lett.*, *17*, 1045.

Yoon, P. H., and A. T. Y. Lui (2005), A class of exact two-dimensional kinetic current sheet equilibria, *J. Geophys. Res.*, *110*, A01202, doi:10.1029/2003JA010308.

M. P. McCarthy and E. C. Whipple, Earth and Space Sciences, University of Washington, Box 351310, Condon Hall Room 310, Seattle, WA 98195, USA. (mccarthy@ess.washington.edu)

L. C. Steinhauer, Redmond Plasma Physics Laboratory, University of Washington, Redmond, WA, USA.